



Ytterbium calcium fluoride waveguide laser

PAVEL LOIKO,¹ RÉMI SOULARD,¹ ESROM KIFLE,² LAUREN GUILLEMOT,¹ GURVAN BRASSE,¹ ABDELMJID BENAYAD,¹ JEAN-LOUIS DOULAN,¹ ALAIN BRAUD,¹ MAGDALENA AGUILÓ,² FRANCESC DÍAZ,² XAVIER MATEOS,² AND PATRICE CAMY^{1,*}

¹Centre de recherche sur les Ions, les Matériaux et la Photonique (CIMAP), UMR 6252 Normandie University, ENSICAEN, UNICAEN, CEA, CNRS, 14000 Caen, France

²Universitat Rovira i Virgili, Departament Química Física i Inorgànica, Física i Cristal·lografia de Materials i Nanomaterials (FiCMA-FiCNA)-EMaS, Campus Sescelades, E-43007 Tarragona, Spain

*patrice.camy@ensicaen.fr

Abstract: Calcium fluoride is a well-known material for optical components. It is also suited for doping with rare-earth ions, e.g., ytterbium ones. Yb:CaF₂ is an efficient gain medium for high-power and ultrashort-pulse bulk lasers around 1 μm. We report on the first Yb:CaF₂ planar waveguide laser. High-optical-quality single-crystalline waveguiding Yb:CaF₂ thin films are grown on bulk CaF₂ substrates by Liquid Phase Epitaxy. The spectroscopic study indicates the predominant coordination of isolated Yb³⁺ ions in trigonal oxygen-assisted sites, C_{3v}(T₂). The optical gain in Yb:CaF₂ waveguide is demonstrated. A 1.4 at.% Yb:CaF₂ planar waveguide laser generated 114 mW at 1037 nm with a slope efficiency of 12.9%. Yb:CaF₂ films are promising for power-scalable waveguide mode-locked lasers and amplifiers.

© 2019 Optical Society of America under the terms of the [OSA Open Access Publishing Agreement](#)

1. Introduction

Calcium fluoride (CaF₂) is a well-known fluoride crystal. It belongs to the cubic class and it is optically isotropic. CaF₂ features good mechanical and thermal properties (thermal conductivity $\kappa = 9.7$ W/mK) [1], a broad transparency range spanning from UV to mid-IR (0.13-10 μm) and a rather low refractive index ($n \sim 1.43$) [2]. As a result, CaF₂ is widely used for manufacturing of optical components (i.e., lenses, optical windows) and it is commercially available. Czochralski (Cz) growth of large-volume CaF₂ crystals is well-developed [3].

CaF₂ has been recognized as a suitable host material for doping with trivalent rare-earth ions and, in particular, ytterbium (Yb³⁺) ones [4]. Yb³⁺ is known for its emission at ~ 1 μm (the ²F_{5/2} → ²F_{7/2} transition). Yb³⁺ features a simple energy-level scheme without unwanted excited-state absorption and energy-transfer upconversion processes and it can be resonantly pumped to the upper laser level, e.g., by high-power InGaAs diode lasers. All of this provides high laser slope efficiencies approaching the Stokes limit and simultaneously weak thermal loading. The typically large Stark splitting of the Yb³⁺ ground-state (²F_{7/2}) leads to broadband emission suitable for mode-locked (ML) lasers.

Yb:CaF₂ crystals thus combine attractive thermo-mechanical properties of the host material and a beneficial spectroscopic behavior of the dopant ions [4]. CaF₂ can be doped with Yb³⁺ ions in desired concentrations (from few to tens at.%) [5]. In this case, Yb³⁺ ions exhibit smooth and broad gain spectra (emission bandwidth of ~ 70 nm) supporting broadband tuning of laser emission [6,7] and generation of sub-100 fs pulses in the ML operation mode [8–10]. At the moment, Yb:CaF₂ crystals are widely used in high-power bulk continuous-wave (CW) and pulsed lasers (including those utilizing the thin-disk geometry [11]) and regenerative amplifiers [12]. Moreover, Yb:CaF₂ is considered as a suitable material for terawatt laser systems [13].

In the recent years, there is a tendency towards the development of compact high-brightness laser sources. Such devices can be realized, e.g., with waveguide (WG) lasers and

amplifiers. They represent one of the key building blocks for integrated photonics. We will consider WGs based on dielectric materials doped with rare-earth ions (RE^{3+}). According to their geometry, optical WGs can be classified into planar and channel ones. A planar WG [14,15] consists of a thin active layer (with a thickness ranging from few μm to hundreds of μm , depending on the material and its deposition method) deposited onto a substrate. The active layer contains the RE^{3+} ions acting as luminescent centers. Optionally, it can be further covered by a cladding in order to enhance the mode confinement, to reduce the WG propagation losses and to protect the WG top surface [16]. The positive refractive index contrast between the layer and the substrate / cladding provides index-guiding of optical modes in the layer in one direction (vertical, perpendicular to the layer plane). This mechanism is much stronger than the possible thermo-optic effects (thermal lensing which strongly affects the mode formation in bulk solid-state lasers). There exist several methods to fabricate waveguiding thin-films, such as Liquid Phase Epitaxy (LPE) [17], molecular beam epitaxy (MBE) [18], pulsed laser deposition (PLD) [19] or reactive co-sputtering [20].

A channel WG consists of a stripe of an active material with a finite cross-section deposited onto the substrate (the so-called surface (ridge) channel WG) or embedded into the substrate / cladding volume (the so-called buried channel WG). The advantage of the channel active WG is the light guiding in both transverse directions leading to symmetric single-transverse-mode output, stronger mode confinement and smaller mode area resulting in lower laser threshold. Surface channel WGs are also suitable for functionalization via the evanescent-field interaction. Channel WGs may be achieved by micro-structuring of the planar structures, e.g., by reactive ion etching [21] or mechanical dicing [22]. Alternatively, they can be directly formed in the volume of the bulk materials, e.g., by ultrafast laser inscription (ULI) [23].

A well-known technology for fabrication of waveguiding films is the Liquid Phase Epitaxy [17]. This technique allows the growing of single-crystalline films with low passive losses [24–26]. The LPE technology has been demonstrated for fluorides materials on the example of tetragonal LiYF_4 [26]. Recently, the LPE growth of rare-earth-dope CaF_2 thin films has also been reported [27,28].

In the present work, we aimed to demonstrate the first $\text{Yb}:\text{CaF}_2$ waveguide laser based on LPE technology which is expected to pave the way towards a new family of CW and ML integrated light sources at $\sim 1 \mu\text{m}$.

Regarding LPE $\text{Yb}:\text{CaF}_2$ waveguiding films, previously, only growth and preliminary spectroscopic characterization were reported [27]. $\text{Er}^{3+}, \text{Yb}^{3+}$ and $\text{Pr}^{3+}, \text{Yb}^{3+}$ -codoped CaF_2 thin films were also grown by molecular beam epitaxy (MBE) [29,30] but no laser operation was reported. In [31], planar and channel (ridge) WGs were fabricated in bulk $\text{Yb}:\text{CaF}_2$ crystals by H^+ ion implantation and their waveguiding and luminescent properties were studied. Very recently, channel WGs were fabricated in $\text{Yb}^{3+}, \text{Na}^+$ -codoped CaF_2 bulk crystal by ULI [32]. Under pumping by a high-brightness laser source at 946 nm, the WG laser generated 174 mW at 1014 nm with an optical-to-optical efficiency of 45.3%. The same method has been also applied to CaF_2 crystals doped with Nd^{3+} ions [33].

2. Fabrication of waveguides

$\text{Yb}:\text{CaF}_2$ single-crystalline thin films were grown by LPE on undoped non-oriented CaF_2 substrates [27]. The double-side laser-grade-polished substrates with dimensions of $20 \times 12 \text{ mm}^2$ and a thickness of 2.0 mm were cut from a bulk CaF_2 crystal grown by the Cz method. As a solvent for LPE growth, calcium chloride (CaCl_2) was used. The phase diagram of the $\text{CaCl}_2 - \text{CaF}_2$ system is shown in Fig. 1. The solvent / solute ($\text{CaCl}_2 / \text{CaF}_2 + \text{YbF}_3$) were taken with an equimolar composition (50 / 50 mol%). YbF_3 (3.6 mol% with respect to CaF_2) was added to ensure Yb^{3+} -doping of the film. The growth was performed in a quartz crucible in a controlled Ar atmosphere. The growth charge was 200 g in weight and the solution was homogenized at 50 °C above the saturation temperature T_s of ~ 820 °C. The growing process

was then performed at the temperatures of 850 – 830 °C with a cooling rate of 0.66 °C/min for a total of 30 min. The substrate dipped into the solution was tilted to ensure more uniform thickness of the film and Yb^{3+} concentration. The resulting film thickness was $\sim 30 \mu\text{m}$. The structure of the films (cubic class, sp. gr. $Fm\bar{3}m$) was confirmed by single-crystal X-ray diffraction.

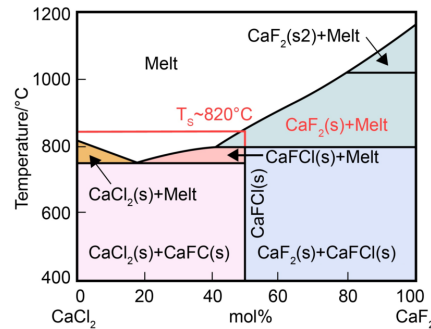


Fig. 1. Phase diagram of the $\text{CaCl}_2 - \text{CaF}_2$ system. The red lines indicate the selected growth conditions, (s) is the solid phase.

Both end-facets of the epitaxy and its top surface were first lapped on a resin plate using micron powders and then polished using a fine powder. The parallelism of the end-facets was better than $5'$ (arcmin) and the flatness of the top surface was about $\lambda/8$. The r.m.s. surface roughness inspected using a confocal microscope (Sensofar, model S-neox) in the interferometric mode was $\sim 5 \text{ nm}$. The end-facets were remained uncoated. The inspection of a polished end-facet with an optical microscope (Olympus BH2-UMA) revealed a good optical quality and uniformity of the $\text{Yb}:\text{CaF}_2$ layers. The resulting layer thickness was $27 \pm 1 \mu\text{m}$. The final length of the planar WG was 10.8 mm. It was non-oriented with respect to principal crystallographic directions.

The refractive index of the $\text{Yb}:\text{CaF}_2$ layer n_{layer} was measured using the Brewster angle technique at $0.633 \mu\text{m}$. The refractive index variation $\Delta n = n_{\text{layer}} - n_{\text{subst}}$ was 5×10^{-3} (for undoped CaF_2 , $n_{\text{subst}} = 1.4289$ at $1 \mu\text{m}$). See Fig. 2.

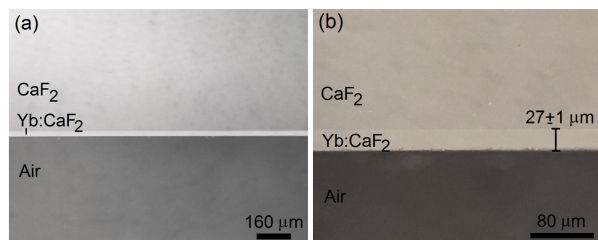


Fig. 2. (a,b) Optical microscope images of the polished end-facet of the $\text{Yb}:\text{CaF}_2 / \text{CaF}_2$ epitaxy.

The actual Yb^{3+} concentration was determined to be $1.4 \pm 0.2 \text{ at.}\%$ ($N_{\text{Yb}} = 3.43 \times 10^{20} \text{ cm}^{-3}$) from small-signal transmission measurements in the WG geometry using a Ti:Sapphire laser. The segregation coefficient $K_{\text{Yb}} = N_{\text{layer}}/N_{\text{solution}}$ was about 0.4.

3. Results and discussion

3.1. Spectroscopy

All the spectroscopic studies were performed at room temperature (RT, 20 °C). The RT absorption, σ_{abs} , and stimulated-emission (SE), σ_{SE} , cross-sections for $\text{Yb}:\text{CaF}_2$ layer are plotted in Fig. 3. The σ_{SE} spectrum was determined using the Füchtbauer-Ladenburg (F-L)

equation [34] using the measured luminescence spectrum and the upper laser level lifetime $\tau_{\text{lum}} = 2.10$ ms (see below). The luminescence spectrum was measured using an optical spectrum analyzer (OSA, Ando AQ-6315E) with a spectral resolution of 0.1 nm. The σ_{abs} spectrum was calculated using the reciprocity method (RM) [35].

At the wavelength of 974.9 nm assigned to the zero-phonon-line transition (ZPL) of Yb^{3+} ions, the maximum $\sigma_{\text{SE}} = 0.70 \times 10^{-20}$ cm² and the corresponding $\sigma_{\text{abs}} = 0.68 \times 10^{-20}$ cm². The full width at half maximum (FWHM) of this absorption peak is 12.9 nm. Yb^{3+} ions represent a quasi-three-level laser scheme. The laser emission is expected at wavelengths longer than the ZPL, where $\sigma_{\text{SE}} = 0.27 \times 10^{-20}$ cm² for a local peak at 1036 nm.

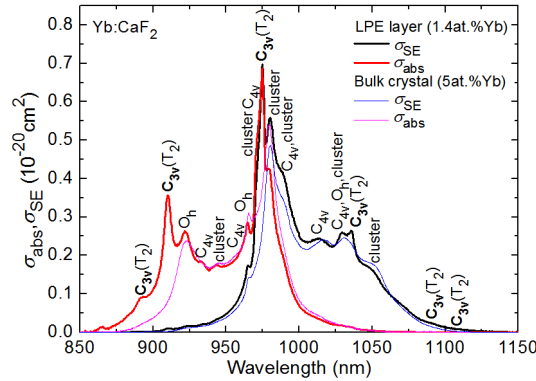


Fig. 3. RT absorption, σ_{abs} , and stimulated-emission (SE), σ_{SE} , cross-sections for 1.4 at.% Yb:CaF₂ LPE-grown layer and the assignment of absorption and emission peaks. The spectra for a bulk 5 at.% Yb:CaF₂ crystal are given for comparison.

In Fig. 3, the absorption and SE cross-section spectra for a bulk 5 at.% Yb:CaF₂ crystal are shown for comparison and they are clearly different from those for the Yb:CaF₂ LPE layer.

To explain this, first, we studied in detail the Yb^{3+} emission around the ZPL, Fig. 4. When Yb^{3+} ions are used as dopant in CaF₂, they replace Ca²⁺ host-forming cations. The excess of charge is compensated by interstitial F⁻ ions forming several kinds of luminescent centers [36]. For low Yb^{3+} doping of <0.1 at.%, the ions are mostly isolated and the centers can be tetragonal (C_{4v}), trigonal (C_{3v}) or cubic (O_h). For higher concentration, Yb^{3+} clusters are formed [37]. This is clear from Fig. 4 where the emission spectra of several bulk Yb:CaF₂ crystals with the doping concentration ranging from 0.05 at.% to 5.5 at.% are compared. For 0.05 at.% Yb^{3+} , the ZPL at ~ 10310 cm⁻¹ is assigned to C_{4v} sites and its weak shoulder at ~ 10370 cm⁻¹ – to the O_h ones. For >0.8 at.% Yb^{3+} , the ZPL at 10201 cm⁻¹ assigned to clusters is dominant. However, for the Yb:CaF₂ LPE layer, the emission spectra are distinct from those for bulk crystals. They contain an intense peak at 10257 cm⁻¹ and weaker features due to the C_{4v} and O_h sites and the clusters which only start to form.

The possible reason for the peak at 10257 cm⁻¹ is the trigonal oxygen-assisted site, C_{3v}(T₂) where the O²⁻ ion substitutes for one of the F⁻ ions in the nearest cubic environment of Yb^{3+} [38]. Such a site is realistic for LPE-grown layers due to the lower growth temperature as compared to the Cz method (CaF₂ melting point: 1418 °C) and a presence of a minor fraction of oxygen in the growth atmosphere which does not lead to formation of an oxyfluoride phase.

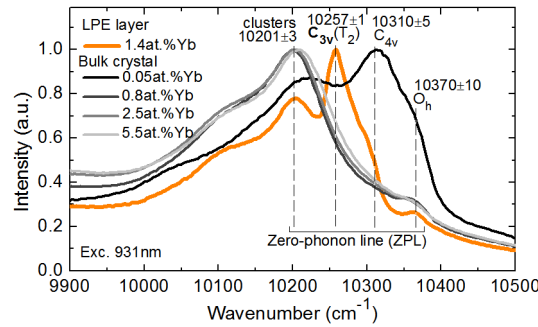


Fig. 4. RT luminescence spectra of bulk Yb:CaF₂ crystals with various doping levels and 1.4 at.% Yb:CaF₂ LPE-grown layer around the zero-phonon line (ZPL) transition of Yb³⁺ ions in various sites. $\lambda_{exc} = 931$ nm.

Assuming a dominant role of C_{3v}(T₂) Yb³⁺ sites with a minor fraction of C_{4v}, O_h and cluster ones for LPE layers, a successful assignment of the absorption and emission peaks is feasible as shown in Fig. 3. The Stark splitting for Yb³⁺ ions entering each of the sites used for this assignment is shown in Fig. 5(a). For the C_{3v}(T₂) site, the partition functions used for the calculation of the absorption cross-sections by RM are $Z_1(^2F_{7/2}) = 1.061$ and $Z_2(^2F_{5/2}) = 1.036$. The coordination of Yb³⁺ ions in the C_{3v}(T₂) site is shown in Fig. 5(b).

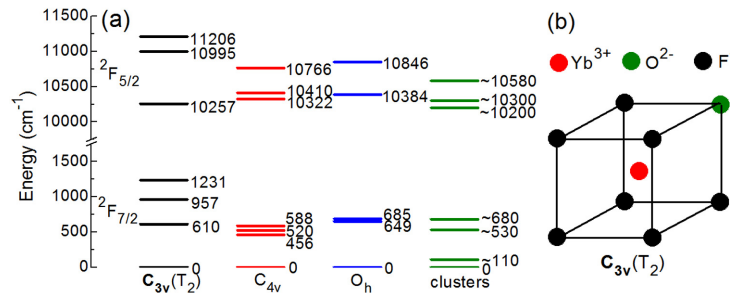


Fig. 5. (a) Stark splitting for Yb³⁺ ions in different sites of CaF₂ crystals after [36,38]; (b) Coordination of Yb³⁺ ion in the C_{3v}(T₂) site [38].

The luminescence decay of Yb³⁺ ions at 1010 nm was studied using a ns optical parametric oscillator (Continuum Horizon) tuned to 930 nm as a pump source, a fast InGaAs photodetector and a 8 GHz Tektronix DSA70804B digital oscilloscope. To reduce the effect of reabsorption (radiation trapping) on the measured decay curves, the pinhole method [39] was applied.

The luminescence decay curves for bulk Yb:CaF₂ crystals and the LPE layer measured using the smallest applied pinhole (diameter: 0.5 mm) are presented in Fig. 6(a). All of them are single-exponential. For bulk crystal with the smallest studied Yb³⁺ doping concentration of 0.05 at.%, the luminescence decay time τ_{lum} is 2.32 ms. With increased Yb³⁺ concentration, the τ_{lum} value slightly changes due to a change of the predominant ion environment (from isolated ions in the C_{4v}, C_{3v} and O_h sites to Yb³⁺ clusters). For the LPE layer, $\tau_{lum} = 2.10$ ms. Due to the small thickness of the LPE layer and relatively low Yb³⁺ concentration, no effect of reabsorption on the measured τ_{lum} values was detected as shown in Fig. 6(b).

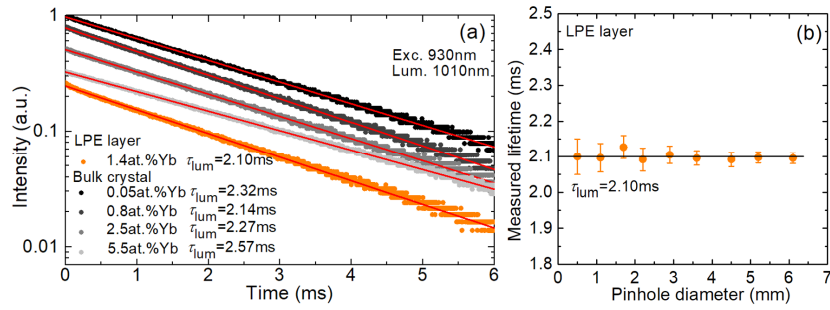


Fig. 6. (a) RT luminescence decay curves 1.4 at.% Yb:CaF₂ LPE-grown layer and bulk Yb:CaF₂ crystals with various doping levels. $\lambda_{\text{exc}} = 930$ nm, $\lambda_{\text{lum}} = 1010$ nm. *Symbols*: experimental data, *lines*: single-exponential fits for the determination of the luminescence lifetime τ_{lum} ; (b) pinhole method evaluation of the reabsorption-free lifetime for the LPE layer.

3.2. Gain measurement

The small-signal (unsaturated) optical gain in the Yb:CaF₂ planar WG was measured by the pump-probe method, Fig. 7. The pump was from a Ti:Sapphire laser (Spectra-Physics, model 3900S) delivering up to 1.8 W at $\lambda_p = 975$ nm. The probe was obtained from a home-made fiber-laser-pumped bulk Yb:CaF₂ laser at $\lambda_s = 1047$ nm. The probe power was limited to 50 mW so that the gain was not saturated by the probe. Both the pump and probe laser sources generated almost diffraction-limited output ($M^2 \approx 1$). Both beams were reshaped with telescopes (a pair of spherical lenses with $f = 50$ mm and 100 mm resulting in a 1:2 magnification) and coupled into the WG by a spherical lens (focal length: $f = 40$ mm). The coupling efficiency for the pump and probe beam was measured to be $\eta_{\text{coupl,P}} = 73 \pm 1\%$ and $\eta_{\text{coupl,S}} = 90 \pm 1\%$, respectively (including the Fresnel loss at the uncoated input WG facet). The position of the focusing lens was adjusted to provide the maximum coupling efficiency for the probe beam.

The population of the Yb³⁺ multiplets under the propagation of the probe and pump beams in the WG was described using the following rate equation:

$$\frac{dN_2}{dt} = -\frac{N_2}{\tau_2} + (\sigma_{\text{abs}}^p N_1 - \sigma_{\text{SE}}^p N_2) I_p - (\sigma_{\text{SE}}^s N_2 - \sigma_{\text{abs}}^s N_1) I_s, \quad (1)$$

where, N_1 and N_2 are the ion densities in the ground-state ($^2F_{7/2}$) and the excited-state ($^2F_{5/2}$), respectively, and $N_1 + N_2 = N_{\text{Yb}} = 3.43 \times 10^{20}$ cm⁻³, t is time (the steady-state case is considered, so that $dN_2/dt = 0$), $\tau_2 = 2.10$ ms is the lifetime of the excited state, $\sigma_{\text{abs}}^p = 0.68 \times 10^{-20}$ cm² and $\sigma_{\text{SE}}^p = 0.70 \times 10^{-20}$ cm² are the absorption and SE cross-sections at the pump wavelength (λ_p), respectively, the cross-sections $\sigma_{\text{abs}}^s = 0.5 \times 10^{-22}$ cm² and $\sigma_{\text{SE}}^s = 0.17 \times 10^{-20}$ cm² are defined at the probe wavelength (λ_s), I_p and I_s are the pump and probe light intensities, respectively, both expressed in photons/(s·cm²).

We assume that both pump and probe beams has a nearly circular Gaussian intensity profile at the input facet of the WG (for the axial coordinate $x = 0$, beam radius: $w_{p(s)}$ ≈ 14 μm). The beams ($M^2 \approx 1$) are index-guided in the vertical direction and they experience a free propagation with a divergence in the horizontal one. The propagation of both beams is considered through the whole length of the WG (10.8 mm) accounting for absorption and SE at the corresponding wavelengths (λ_p and λ_s) and yielding the pump and probe powers at the output facet.

The probe wavelength used for the gain measurements (1047 nm) was determined by the used source (the Yb:CaF₂ laser) and it is longer than that of the Yb:CaF₂ WG laser (~ 1036 nm, Section 3.4). According to the determined transition cross-section of Yb³⁺ ions in CaF₂ layers, see Fig. 3, the gain is higher at 1047 nm for low inversion because of smaller

reabsorption loss while it is higher at 1036 nm for high inversion (see the gain curves in Section 3.4).

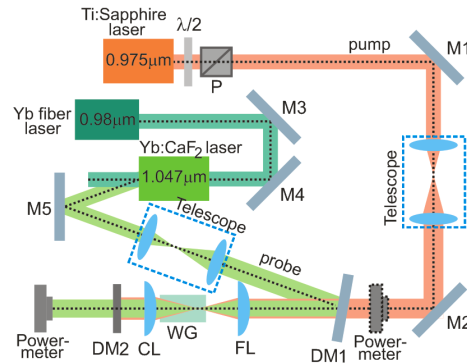


Fig. 7. Scheme of the set-up for gain measurements in planar Yb:CaF₂ WG: $\lambda/2$ – half-wave plate, P – Glan-Taylor polarizer, M1-M5 – flat highly-reflective folding mirrors, DM1 and DM2 – dichroic mirrors, FL – focusing lens, CL – collimating lens, WG – waveguide.

The measured pump absorption η_{abs} is shown in Fig. 8(a). It decreased with pump power due to the depopulation of the Yb³⁺ ground-state (absorption bleaching). The net gain $g_{\text{net}} = g_{\text{rel}} - \delta_{\text{abs}} - \delta_{\text{loss}}$, where $g_{\text{rel}} = 10 \log_{10}(P_{\text{S,P}}/P_{\text{S,P}=0})$ is the relative gain ($P_{\text{S,P}}$ is the transmitted signal for a given launched pump power $P_{\text{coupl,P}} = \eta_{\text{coupl,P}} P_{\text{inc}}$, $P_{\text{S,P}=0}$ is the transmitted signal for zero pump power $P_{\text{inc}} = 0$), δ_{abs} is the small-signal Yb³⁺ absorption loss at λ_{S} , and δ_{loss} is the WG passive (propagation) loss, see below. The maximum measured net gain was 0.40 ± 0.06 dB/cm, see Fig. 8(b). Both η_{abs} and g_{net} were calculated using a rate-equation model accounting for spatial profiles of the pump and signal beams as explained above. The results show a good agreement with the experiment, Fig. 8.

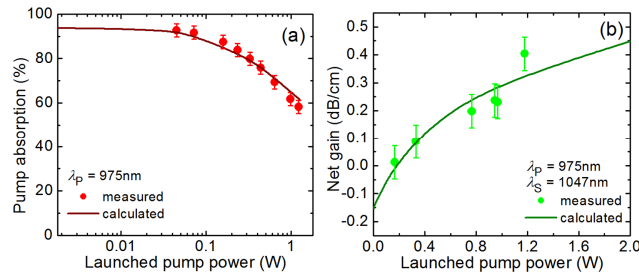


Fig. 8. Yb:CaF₂ planar WG: measured and calculated (a) pump absorption at $\lambda_{\text{p}} = 975$ nm; (b) small-signal net gain at $\lambda_{\text{S}} = 1047$ nm.

3.3. Laser setup

The scheme of the laser set-up is shown in Fig. 9(a). The pump was still the continuous-wave (CW) Ti:Sapphire laser tuned to $\lambda_{\text{p}} = 975$ nm. The pump beam was attenuated with a rotatable $\lambda/2$ plate and a Glan-Taylor polarizer and focused into the WG by an uncoated spherical CaF₂ plano-convex lens (Thorlabs, LA5370, $f = 40$ mm, transmission: $T = 96.9\%$) resulting in a pump spot diameter $2w_{\text{p}}$ of $35 \mu\text{m}$ and $\eta_{\text{coupl}} = 73 \pm 1\%$. The pump absorption at the laser threshold η_{abs} was determined separately for each OC from Fig. 8(a). The pumped Yb:CaF₂ WG exhibited blue upconversion luminescence due to the impurity Tm³⁺ ions present in the YbF₃ reagent, Fig. 9(b).

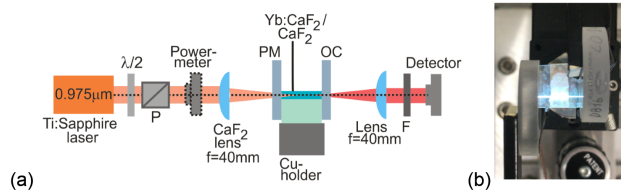


Fig. 9. (a) Scheme of the laser set-up: P – Glan-Taylor polarizer, PM – pump mirror, OC – output coupler, F – cut-off filter; (b) photograph of the pumped Yb:CaF₂ WG laser.

The laser cavity was formed by a flat pump mirror (PM) coated for high transmission (HT) at 0.88-0.98 μm ($T = 96.2\%$ at 975 nm) and for high reflection (HR) at 1.02-1.10 μm , and a set of flat output couplers (OCs) having a transmission T_{OC} of 1%, 2%, 5% and 10% at the laser wavelength. Both PM and OC were placed close to the WG end-facets with minimum air gaps. No index-matching liquid was used. The epitaxy was mounted on a Cu-holder using a silver paste and it was passively-cooled.

The laser spectra were measured using the OSA. To determine the laser beam profile at the output facet of the WG, the laser output was first collimated using a spherical CaF₂ bi-convex lens (Thorlabs, LB5766, $f = 15$ mm) and the 2D profile was captured using a FIND-R-SCOPE near-IR camera (model 85726). The camera was calibrated by illuminating the WG with a near-IR light source. The M^2 parameter of the laser beam was measured in the far-field. The laser output was collimated and focused using a pair of 40 mm focal length lenses and the diameter of the laser mode in the horizontal and vertical planes was determined at the $1/e^2$ level using a CCD camera (DataRay, BladeCam-XHR).

3.4. Laser experiment

The input-output dependencies for the Yb:CaF₂ planar WG laser are shown in Fig. 10. They are linear showing minor thermal effects. The maximum output power reached 114 mW at 1037 nm with a slope efficiency η of 12.9% (vs. the absorbed pump power P_{abs}). The laser threshold was at $P_{\text{abs}} = 0.24$ W. The optical-to-optical efficiency vs. the incident power was 6%. The power scaling was limited by the available pump power. The WG propagation losses were estimated from the Findlay-Clay analysis as $\delta_{\text{loss}} = 0.14 \pm 0.05$ dB/cm. The laser emission was unpolarized.

The typical laser emission spectra are shown in Fig. 11(a). For the example of 10% OC, the FWHM of the emission line is about 0.5 nm. For all the OCs, the laser emission occurred around 1036 nm. This agrees well with the gain cross-section, $\sigma_g = \beta\sigma_{\text{SE}} - (1 - \beta)\sigma_{\text{abs}}$, spectra for Yb³⁺ ions in the studied layers, Fig. 11(b). For the studied OCs, the inversion ratios $\beta = N_2(^2F_{5/2})/N_{\text{Yb}}$ averaged over the WG length are in the range 0.1-0.2. The corresponding gain spectra feature a local peak at ~ 1036 nm being specific for the C_{3v}(T₂) Yb³⁺ sites.

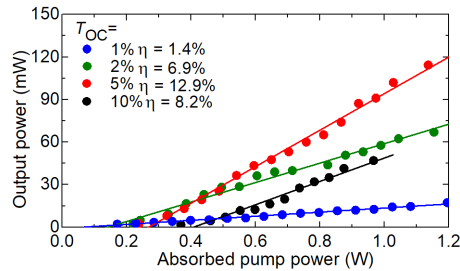


Fig. 10. Input-output dependences for the Ti:Sapphire-pumped Yb:CaF₂ planar WG laser, η – slope efficiency.

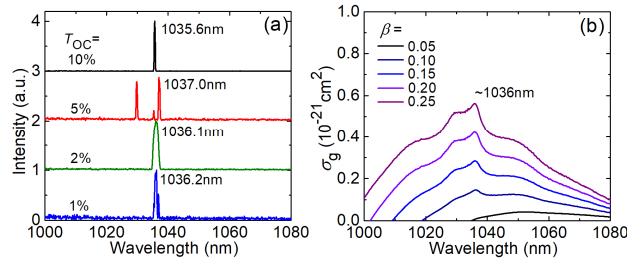


Fig. 11. (a) Typical laser emission spectra for the Yb:CaF₂ planar WG laser, measured at $P_{\text{abs}} \sim 0.6$ W; (b) gain cross-section, $\sigma_g = \beta\sigma_{\text{SE}} - (1 - \beta)\sigma_{\text{abs}}$, spectra for different inversion ratios $\beta = N_2(^2F_{5/2})/N_{\text{Yb}}$.

As explained in Section 3.3, we have determined the laser mode profile corresponding to the output facet of the WG. The 2D mode profile is shown in Fig. 12(a). It has a shape of a stripe extended along the horizontal direction which is characteristic for planar WGs. In Fig. 12(b), the 1D intensity profiles are also plotted. According to the high measured refractive index variation between the active layer and the substrate Δn , the planar Yb:CaF₂ WG can support several modes in the vertical direction (y). However, the corresponding 1D intensity profile is nearly Gaussian along the y -axis (mode diameter at the $1/e^2$ level: $2w_L = 22 \mu\text{m}$, goodness of the Gaussian fit: $R^2 > 0.99$). In the horizontal (unguided) direction (z), the 1D intensity profile has additional spatial artifacts resulting from possible excitation of higher-order modes. The mode diameter $2w_L = 218 \mu\text{m}$ (goodness of the Gaussian fit: $R^2 = 0.97$).

To understand better the mechanism of mode formation, we measured the beam quality factors (M^2) along both the y and z directions. Note that due to much stronger mode divergence along the fast (y) axis, the laser mode in the far-field appears as a vertically oriented stripe. The evaluation of the M^2 parameters for the optimum 5% OC and almost maximum studied $P_{\text{abs}} = 1.1$ W is shown in Figs. 12(c) and 12(d), following the ISO-standard procedure [40]. The determined beam quality factors are $M_y^2 = 1.0 \pm 0.1$ and $M_z^2 = 1.2 \pm 0.1$. The small M^2 parameter and relatively clear 1D intensity mode profile in the horizontal direction suggest that the gain guiding mechanism is responsible for the mode formation in the Yb:CaF₂ WG laser (the mode size is limited by absorption in the unpumped regions of the WG).

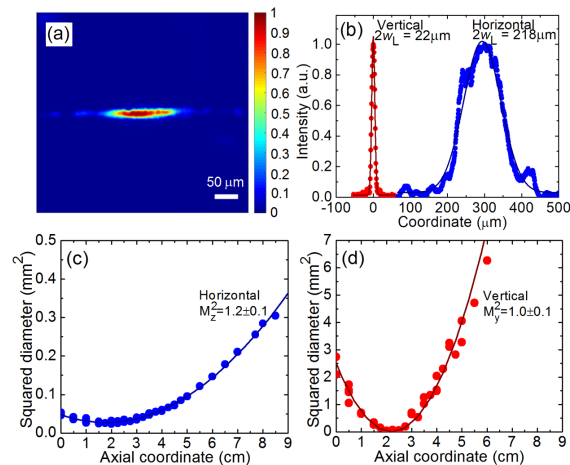


Fig. 12. Evaluation of beam quality of the laser output from the Yb:CaF₂ planar WG laser: (a,b) near-field beam profile: (a) 2D profile; (b) 1D profiles in the horizontal and vertical directions, *symbols*: experimental data, *curves* – their Gaussian fits (at $P_{\text{abs}} = 0.6$ W); (c,d) evaluation of the M^2 factors in the far-field in (c) the horizontal and (d) vertical directions:

symbols – squared measured diameters of the laser mode, *curves* – their parabolic fits (at $P_{\text{abs}} = 1.1$ W). $T_{\text{oc}} = 5\%$.

The grown films are suitable for further fabrication of channel WGs, e.g., diamond-saw-dicing [41] with still low propagation losses of <0.3 dB/cm. A reduction of lateral size of WGs down to few μm is expected to provide single-mode operation. Such Yb:CaF₂ channel WGs combined with a saturable absorber mirror (SAM) replacing one of the cavity mirrors may bring exciting possibilities for development of compact high-repetition-rate (GHz-range, as dictated by the cavity length) ultrashort-pulse oscillators at ~ 1 μm [42,43]. As a SAM, semiconductor ones [42] or those based on 2D materials such as graphene [43] can be implemented. Yb:CaF₂ is particularly suitable for ML applications due to its broadband emission properties.

4. Conclusion

Liquid phase epitaxy grown Yb:CaF₂ single-crystalline thin films are promising for the development of WG lasers and amplifiers around 1 μm . The potential of Yb:CaF₂ LPE technology is determined by (i) high availability and well-developed growth method for undoped CaF₂ used for substrates, (ii) good thermo-mechanical properties of CaF₂ making it suitable for power-scalable designs, (iii) high refractive-index contrast in Yb³⁺-doped films without the use of additional passive ions serving as refractive index modifiers, and (iv) attractive spectroscopic properties of Yb³⁺ ions in CaF₂. In the present work, we report on the first Yb:CaF₂ LPE-based *waveguide* laser delivering 114 mW at 1037 nm with a slope efficiency of 12.9% and featuring low WG propagation losses of 0.14 ± 0.05 dB/cm. The optical gain in such a planar WG is measured at 1057 nm.

Further improvement of the fabrication technology should focus on the reduction of the WG propagation losses. The growth procedure should also be optimized to reduce the oxygen content in the growth atmosphere and to allow higher Yb³⁺ doping levels. According to the estimated lattice mismatch for Yb:CaF₂ / CaF₂ epitaxies, doping with up to 5 at.% of Yb³⁺ ions should still ensure good optical quality of the grown layers. Both oxygen presence and Yb³⁺ concentration are however expected to affect the predominant ion coordination.

Funding

European Community Funds (FEDER); Normandie Region; Spanish Government (MAT2016-75716-C2-1-R, TEC 2014-55948-R); Generalitat de Catalunya (2014SGR1358).

Acknowledgment

This work was supported by the European Community funds FEDER and the Normandie region.

References

1. G. A. Slack, "Thermal conductivity of CaF₂, MnF₂, CoF₂, and ZnF₂ crystals," *Phys. Rev.* **122**(5), 1451–1464 (1961).
2. I. H. Malitson, "A redetermination of some optical properties of calcium fluoride," *Appl. Opt.* **2**(11), 1103–1107 (1963).
3. K. Nassau, "Application of the Czochralski method to divalent metal fluorides," *J. Appl. Phys.* **32**(10), 1820–1821 (1961).
4. F. Druon, S. Ricaud, D. N. Papadopoulos, A. Pellegrina, P. Camy, J. L. Doualan, R. Moncorgé, A. Courjaud, E. Mottay, and P. Georges, "On Yb:CaF₂ and Yb:SrF₂: review of spectroscopic and thermal properties and their impact on femtosecond and high power laser performance," *Opt. Mater. Express* **1**(3), 489–502 (2011).
5. M. Ito, C. Goutaudier, Y. Guyot, K. Lebbou, T. Fukuda, and G. Boulon, "Crystal growth, Yb³⁺ spectroscopy, concentration quenching analysis and potentiality of laser emission in Ca_{1-x}Yb_xF_{2+x}," *J. Phys. Condens. Matter* **16**(8), 1501–1521 (2004).
6. A. Lucca, M. Jacquemet, F. Druon, F. Balembois, P. Georges, P. Camy, J. L. Doualan, and R. Moncorgé, "High-power tunable diode-pumped Yb³⁺:CaF₂ laser," *Opt. Lett.* **29**(16), 1879–1881 (2004).

7. A. Jouini, A. Brenier, Y. Guyot, G. Boulon, H. Sato, A. Yoshikawa, K. Fukuda, and T. Fukuda, "Spectroscopic and laser properties of the near-infrared tunable laser material Yb³⁺-doped CaF₂ crystal," *Cryst. Growth Des.* **8**(3), 808–811 (2008).
8. A. Lucca, G. Debourg, M. Jacquemet, F. Druon, F. Balembois, P. Georges, P. Camy, J. L. Doualan, and R. Moncorgé, "High-power diode-pumped Yb³⁺:CaF₂ femtosecond laser," *Opt. Lett.* **29**(23), 2767–2769 (2004).
9. G. Machinet, P. Seviliano, F. Guichard, R. Dubrasquet, P. Camy, J.-L. Doualan, R. Moncorgé, P. Georges, F. Druon, D. Descamps, and E. Cormier, "High-brightness fiber laser-pumped 68 fs-2.3 W Kerr-lens mode-locked Yb:CaF₂ oscillator," *Opt. Lett.* **38**(20), 4008–4010 (2013).
10. F. Pirzio, S. D. Di Dio Cafiso, M. Kemnitzer, F. Kienle, A. Guandalini, J. Aus der Au, and A. Agnesi, "65-fs Yb:CaF₂ laser mode-locked by semiconductor saturable absorber mirror," *J. Opt. Soc. Am. B* **32**(11), 2321–2325 (2015).
11. B. Dannecker, X. Délen, K. S. Wentsch, B. Weichelt, C. Hönninger, A. Voss, M. A. Ahmed, and T. Graf, "Passively mode-locked Yb:CaF₂ thin-disk laser," *Opt. Express* **22**(19), 22278–22284 (2014).
12. S. Ricaud, F. Druon, D. N. Papadopoulos, P. Camy, J.-L. Doualan, R. Moncorgé, M. Delaigue, Y. Zaouter, A. Courjaud, P. Georges, and E. Mottay, "Short-pulse and high-repetition-rate diode-pumped Yb:CaF₂ regenerative amplifier," *Opt. Lett.* **35**(14), 2415–2417 (2010).
13. M. Siebold, M. Hornung, R. Boedefeld, S. Podleska, S. Klingebiel, C. Wandt, F. Krausz, S. Karsch, R. Uecker, A. Jochmann, J. Hein, and M. C. Kaluza, "Terawatt diode-pumped Yb:CaF₂ laser," *Opt. Lett.* **33**(23), 2770–2772 (2008).
14. J. I. Mackenzie, "Dielectric solid-state planar waveguide lasers: a review," *IEEE J. Sel. Top. Quantum Electron.* **13**(3), 626–637 (2007).
15. C. Grivas, "Optically pumped planar waveguide lasers, part I: fundamentals and fabrication techniques," *Prog. Quantum Electron.* **35**(6), 159–239 (2011).
16. D. P. Shepherd, S. J. Hettrick, C. Li, J. I. Mackenzie, R. J. Beach, S. C. Mitchell, and H. E. Meissner, "High-power planar dielectric waveguide lasers," *J. Phys. D Appl. Phys.* **34**(16), 2420–2432 (2001).
17. B. Ferrand, B. Chambaz, and M. Couchaud, "Liquid phase epitaxy: A versatile technique for the development of miniature optical components in single crystal dielectric media," *Opt. Mater.* **11**(2–3), 101–114 (1999).
18. R. A. McFarlane, M. Lui, and D. Yap, "Rare earth doped fluoride waveguides fabricated using molecular beam epitaxy," *IEEE J. Sel. Top. Quantum Electron.* **1**(1), 82–91 (1995).
19. J. A. Grant-Jacob, S. J. Beecher, T. L. Parsonage, P. Hua, J. I. Mackenzie, D. P. Shepherd, and R. W. Eason, "An 11.5 W Yb:YAG planar waveguide laser fabricated via pulsed laser deposition," *Opt. Mater. Express* **6**(1), 91–96 (2016).
20. E. H. Bernhardt, H. A. G. M. van Wolferen, K. Wörhoff, R. M. de Ridder, and M. Pollnau, "Highly efficient, low-threshold monolithic distributed-Bragg-reflector channel waveguide laser in Al₂O₃:Yb³⁺," *Opt. Lett.* **36**(5), 603–605 (2011).
21. D. Geskus, S. Aravazhi, C. Grivas, K. Wörhoff, and M. Pollnau, "Microstructured KY(WO₄)₂:Gd³⁺, Lu³⁺, Yb³⁺ channel waveguide laser," *Opt. Express* **18**(9), 8853–8858 (2010).
22. E. Kifle, P. Loiko, U. Griebner, V. Petrov, P. Camy, A. Braud, M. Aguiló, F. Díaz, and X. Mateos, "Diamond saw dicing of thulium channel waveguide lasers in monoclinic crystalline films," *Opt. Lett.* **44**(7), 1596–1599 (2019).
23. F. Chen and J. R. V. de Aldana, "Optical waveguides in crystalline dielectric materials produced by femtosecond-laser micromachining," *Laser Photonics Rev.* **8**(2), 251–275 (2014).
24. D. Pelenc, B. Chambaz, I. Chartier, B. Ferrand, C. Wyon, D. P. Shepherd, D. C. Hanna, A. C. Large, and A. C. Tropper, "High slope efficiency and low threshold in a diode-pumped epitaxially grown Yb:YAG waveguide laser," *Opt. Commun.* **115**(5–6), 491–497 (1995).
25. Y. E. Romanyuk, C. N. Borca, M. Pollnau, S. Rivier, V. Petrov, and U. Griebner, "Yb-doped KY(WO₄)₂ planar waveguide laser," *Opt. Lett.* **31**(1), 53–55 (2006).
26. W. Bolaños, F. Starecki, A. Braud, J.-L. Doualan, R. Moncorgé, and P. Camy, "2.8 W end-pumped Yb³⁺:LiYF₄ waveguide laser," *Opt. Lett.* **38**(24), 5377–5380 (2013).
27. A. Peña, P. Camy, A. Benayad, J.-L. Doualan, C. Maurel, M. Olivier, V. Nazabal, and R. Moncorgé, "Yb:CaF₂ grown by liquid phase epitaxy," *Opt. Mater.* **33**(11), 1616–1620 (2011).
28. S. Renard, P. Camy, J. L. Doualan, R. Moncorgé, M. Couchaud, and B. Ferrand, "Tm³⁺:CaF₂ planar waveguides grown by liquid phase epitaxy on CaF₂ substrates showing signal enhancement at 1.92 μm," *Opt. Mater.* **28**(11), 1289–1291 (2006).
29. E. Daran, R. Legros, P. Pernas, and C. Fontaine, "Er–Yb codoped CaF₂ thin films grown by molecular beam epitaxy," *J. Appl. Phys.* **81**(2), 679–684 (1997).
30. F. Lahoz, E. Daran, G. Lifante, T. Balaji, and A. Muñoz-Yagüe, "CaF₂:Yb³⁺+Pr³⁺ codoped waveguides grown by molecular beam epitaxy for 1.3 μm applications," *Appl. Phys. Lett.* **74**(8), 1060–1062 (1999).
31. V. Petit, P. Moretti, P. Camy, J. L. Doualan, and R. Moncorgé, "Active waveguides produced in Yb³⁺:CaF₂ by H⁺ implantation for laser applications," *J. Alloys Compd.* **451**(1–2), 68–70 (2008).
32. Y. Ren, C. Cheng, Y. Jia, Y. Jiao, D. Li, M. D. Mackenzie, A. K. Kar, and F. Chen, "Switchable single-dual-wavelength Yb,Nd:CaF₂ waveguide lasers operating in continuous-wave and pulsed regimes," *Opt. Mater. Express* **8**(6), 1633–1641 (2018).
33. R. Li, W. Nie, Q. Lu, C. Cheng, Z. Shang, J. R. Vázquez de Aldana, and F. Chen, "Femtosecond-laser-written superficial cladding waveguides in Nd:CaF₂ crystal," *Opt. Laser Technol.* **92**, 163–167 (2017).

34. B. Aull and H. Jenssen, "Vibronic interactions in Nd:YAG resulting in nonreciprocity of absorption and stimulated emission cross sections," *IEEE J. Quantum Electron.* **18**(5), 925–930 (1982).
35. S. A. Payne, L. L. Chase, L. K. Smith, W. L. Kway, and W. F. Krupke, "Infrared cross-section measurements for crystals doped with Er^{3+} , Tm^{3+} , and Ho^{3+} ," *IEEE J. Quantum Electron.* **28**(11), 2619–2630 (1992).
36. V. Petit, P. Camy, J.-L. Doualan, X. Portier, and R. Moncorgé, "Spectroscopy of $\text{Yb}^{3+}:\text{CaF}_2$: from isolated centers to clusters," *Phys. Rev. B Condens. Matter Mater. Phys.* **78**(8), 085131 (2008).
37. B. Lacroix, C. Genevois, J. L. Doualan, G. Brasse, A. Braud, P. Ruterana, P. Camy, E. Talbot, R. Moncorgé, and J. Margerie, "Direct imaging of rare-earth ion clusters in $\text{Yb}:\text{CaF}_2$," *Phys. Rev. B Condens. Matter Mater. Phys.* **90**(12), 125124 (2014).
38. M. L. Falin, K. I. Gerasimov, V. A. Latypov, A. M. Leushin, H. Bill, and D. Lovy, "EPR and optical spectroscopy of Yb^{3+} ions in CaF_2 and SrF_2 ," *J. Lumin.* **102–103**, 239–242 (2003).
39. H. Kühn, S. T. Fredrich-Thornton, C. Kränkel, R. Peters, and K. Petermann, "Model for the calculation of radiation trapping and description of the pinhole method," *Opt. Lett.* **32**(13), 1908–1910 (2007).
40. Lasers and laser-related equipment—test methods for laser beam widths, divergence angles and beam propagation ratios—part 1: stigmatic and simple astigmatic beams, ISO 11146–11147 (2005).
41. P. Loiko, R. Souldard, G. Brasse, J. L. Doualan, B. Guichardaz, A. Braud, A. Tyazhev, A. Hideur, and P. Camy, "Watt-level $\text{Tm}:\text{LiYF}_4$ channel waveguide laser produced by diamond saw dicing," *Opt. Express* **26**(19), 24653–24662 (2018).
42. A. Choudhary, A. A. Lagatsky, P. Kannan, W. Sibbett, C. T. A. Brown, and D. P. Shepherd, "Diode-pumped femtosecond solid-state waveguide laser with a 4.9 GHz pulse repetition rate," *Opt. Lett.* **37**(21), 4416–4418 (2012).
43. A. G. Okhrimchuk and P. A. Obratsov, "11-GHz waveguide Nd:YAG laser CW mode-locked with single-layer graphene," *Sci. Rep.* **5**, 11172 (2015).